Phys. Status Solidi A **208**, No. 6, 1246–1251 (2011) / **DOI** 10.1002/pssa.201000991

physica status solidi a
www.pss-a.com
applications and materials science

Grain boundary electrochemistry of β-type Nb–Ti alloy using a scanning droplet cell

Michael Teka Woldemedhin[1,2], Dierk Raabe[2], and Achim Walter Hassel[*,1,2]

[1] Institute for Chemical Technology of Inorganic Materials, Johannes Kepler University, Altenberger Str. 69, 4040 Linz, Austria
[2] Max-Planck-Institut für Eisenforschung GmbH, Max Planck Str. 1, 40237 Düsseldorf, Germany

Received 15 September 2010, revised 29 December 2010, accepted 11 January 2011
Published online 18 May 2011

Keywords biomaterials, anodic oxides, cyclic voltammetry, grain boundary, Mott–Schottky analysis

[*] Corresponding author: e-mail hassel@elchem.de, Phone: +43 732 2468 8703, Fax: +43 732 2468 8905

Localized oxide spots were grown at the grain boundaries of a technically relevant 30 at.% Nb–Ti β-type titanium alloy to study the local electrochemical response. The grain boundaries selected were combinations of grains having different orientations and grain boundary angle. Crystallographic information of the grains and boundary angles were revealed by electron back scattering diffraction (EBSD) technique. Cyclic voltammetry is the electrochemical technique used to grow the oxides starting from 0 V and increasing the potential in steps of 1 V till 8 V at a scan rate of 100 mV s^{-1} in an acetate buffer of pH 6.0. Electrochemical impedance spectroscopy was used to investigate the electrical properties of the oxide/electrolyte interface in the frequency range between 100 kHz and 100 mHz. Important oxide parameters such as formation factor and dielectric number were determined from these measurements. Significant differences were observed for different grain boundaries. The semiconducting properties of the oxides at the grain boundaries were assessed by using Mott–Schottky analysis on a potentiostatically grown oxide. All the oxides showed n-type semiconducting properties where the donor concentration varies with the grain boundaries mentioned above. A flat band potential -0.25 ± 0.02 V versus standard hydrogen electrode is more or less the same for all the boundaries studied.

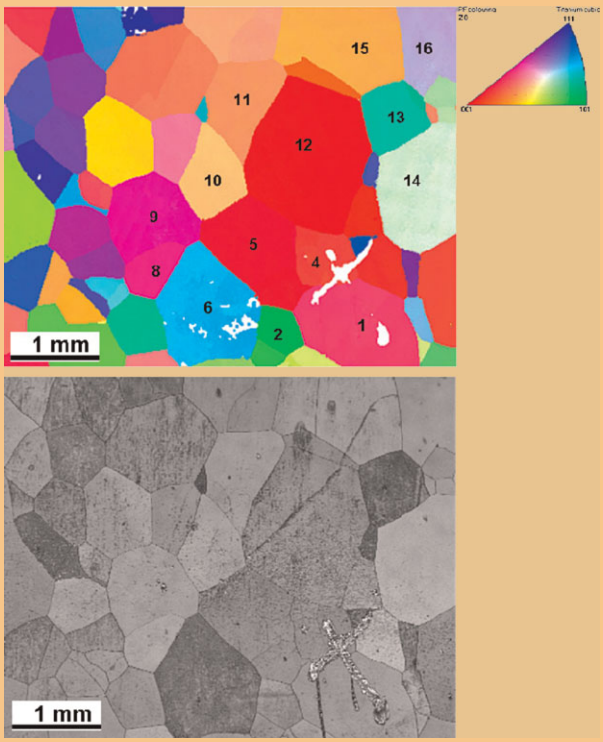

1 Introduction Excellent corrosion resistance coupled with very low toxicity level against osteoblastic cells makes β-type titanium alloys a premium choices over the conventional α-Ti and α–β titanium alloys for applications as biomaterials [1, 2]. Moreover β-Ti alloys have improved mechanical properties such as wear resistance, excellent cold and hot formability and low modulus of elasticity due to solid solution and second phase hardening while preserving the light weight characteristics of titanium [3]. The latter is an important property for load bearing surgical implants intended to be used in place of bone. By using such kind of alloys the mismatch in stiffness between the surgical implant and the surrounding tissue can be reduced. Numerically, the human cortical bone has a

modulus of elasticity around 20 GPa which is much lower than the 100–110 GPa value of conventional titanium alloys. By using β-type titanium alloys this value is reduced significantly to 60 GPa [4, 5]. The reduced mismatch in stiffness minimizes many undesired effects at the bone-implant system such as bone decay as a consequence of abrasion, premature implant failure and infection due to wear debris transport through biological fluids [4, 6].

Unlike the conventional α-type titanium alloys which crystallize in hexagonal closed packed structure, β-type alloys crystallize in a body centred cubic crystal structure. These types of alloys are stabilized for applications at room temperature by alloying them with β-stabilizing elements namely Nb, Mo and Ta [6, 7].

The corrosion resistance of the β-type titanium alloys is attributed to the formation of a stable and dense passive film which protects the bare material underneath from corroding [8, 9]. Nb–Ti (30 at.%) is one type of the β-Ti alloys which is a potential candidate for applications as a biomaterial [10, 11]. The passivity and electronic properties of the mixed oxide grown on macroscopic surfaces of this alloy were studied earlier [12] where no side reactions were observed during oxide growth and the oxide proved to be a perfect dielectric material. Furthermore the dependence of the local electrochemical response of the single grains of 30 at.% Nb–Ti alloy on the crystallographic orientation was studied using a scanning droplet cell. The single grains also exhibited excellent passivity with oxide formation being the sole process in which the oxide thickness is increasing with applied potential. No oxygen evolution was noticed in any of the grains of 30 at.% Nb alloy-Ti, a behaviour different from α-Ti alloys. However, oxide parameters such as oxide formation factor, dielectric number and donor concentration depend on the crystallographic orientation of the substrate grains on which the microelectrochemical measurements were carried out [13]. But the microstructure of polycrystalline materials consists not only of grains but also of grain boundaries. Grain boundary is an important element of the microstructure of a polycrystalline sample where grains of different orientations form an interface which affects the physical and chemical properties such as intergranular fracture, segregation and corrosion [14]. Such kind of local mismatch in orientation can form an interface with unique local surface properties regarding atomic structure and energy. As a result surface properties which might be affected by grain orientation, vacancies and other defects may show different properties at the grain boundaries. Solute segregation, precipitation, embrittlement and corrosion can be resulting properties to name only a few [15]. Thus a comprehensive picture about the corrosion resistance and passivation behaviour of a material can only be obtained without sidelining the effect that grain boundaries might have in dictating the overall electrochemical response. Having these aspects in mind microelectrochemical measurements were carried out at the grain boundaries of a 30 at.% Nb–Ti β-Ti alloy to study the local electrochemical response by means of the scanning droplet cell.

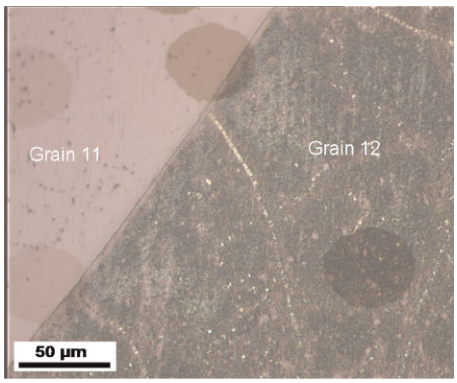

Figure 1 (online colour at: www.pss-a.com) Optical micrograph of oxide spots at a grain boundary of 30 at.% Nb–Ti sample.

2 Experimental

2.1 Sample preparation A β-type 30 at.% Nb–Ti sample was ground with silicon carbide paper till 2500 grit and polished with silica slurry to a mirror finish. The sample surface preparation was finalized by electropolishing potentiostatically at 8 V in 3 M methanolic sulphuric acid solution at −22 °C [16]. The sample surface was rinsed with distilled water and cleaned with ethanol in an ultrasonic bath after each procedure.

2.2 Electrochemical experiments Oxide spots were grown at different grain boundaries varying in grain boundary angles and crystallographic orientation combinations of 30 at.% Nb–Ti sample using a scanning droplet cell to study the local electrochemical response as shown in Fig. 1. The oxides were grown by scanning the potential at a rate of 100 mV s^{-1} from 0 V in steps of 1 V till 8 V using cyclic voltammetry technique in an acetate buffer of pH 6.0. Electrochemical impedance measurements were carried out in a frequency range of 100 kHz to 100 mHz right after each potential sweep to study the electronic properties of the oxides grown. The semiconducting properties of the oxides were studied using Mott–Schottky analysis on an oxide grown potentiostatically at 3 V for 1000 s. All potentials in this paper refer to standard hydrogen electrode (SHE) potential.

2.3 Experimental set up Figure 2 shows the schematic illustration of the scanning droplet cell, the microcell used in all of the experiments [17, 18]. The scanning droplet cell was mounted on a force sensor (KD45 2N, ME-Messsysteme) for controlling precisely the amount of force applied by the cell tip on the sample surface. This is the crucial part in setting up the experiment for it helps to maintain the wetted area constant for successive measurements on the sample surface. The other end of the force sensor is fixed on a 3D scanner for the spatial movement of the cell tip across the sample surface. Two live cameras were used to control the vertical and lateral movement of the cell tip in relation to the sample surface. Precise amount of

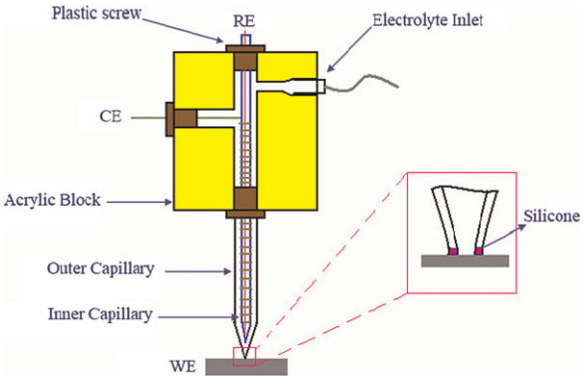

Figure 2 (online colour at: www.pss-a.com) Schematic diagram of the scanning droplet cell.

electrolyte is injected from a 100 μl syringe into the scanning droplet cell with the help of a computer controlled microsyringe injector (Micro 4, WPI). The whole set up described so far was mounted on a bread board which is suspended on shock absorber to maintain constant contact of the cell tip with the sample surface. A Princeton Applied Research Potentiostat/Galvanostat model 283 coupled with a frequency response analyser (S5720C, NF Electronic Instruments) was used in all experiments.

2.4 Electron back scattering diffraction Crystallographic orientation of the grains and grain boundary angles were determined from electron back scattering diffraction (EBSD) scans shown on Fig. 3 of the 30 at.% Nb–Ti sample carried out after electropolishing and before the microelectrochemical measurements. The EBSD analysis was carried out in a field emission scanning electron microscope (Zeiss 1540XB) having an additional EBSD unit. An acceleration electron beam of 20 keV was focused on a small area of the sample tilted at 70°. The scratch with a shape of a cross at the very right bottom corner serves as reference point to address specific grain boundaries.

2.5 Atomic force microscopy The topography of the grain boundaries was studied by atomic force microscopy (AFM, Asylum Research MFP3D). The experiments were carried out in non-contact mode using a microcantilever with a force constant of 2 N m^{-1} and a commercial silicon tip (Olympus).

3 Results and discussion

3.1 Cyclic voltammetry Figure 4 shows the cyclic voltammogramms obtained from the local electrochemical measurements carried out on different grain boundaries of the 30 at.% Nb–Ti sample. All grain boundaries showed very small current for the first cycle of the potential scan due to the thickness of the native oxide covering the surface after air passivation. Significant increase in current is observed starting from the second cycle onward. An overshoot in current is observed in the second cycle which broadens and later disappears after the third cycle due to a delay in the

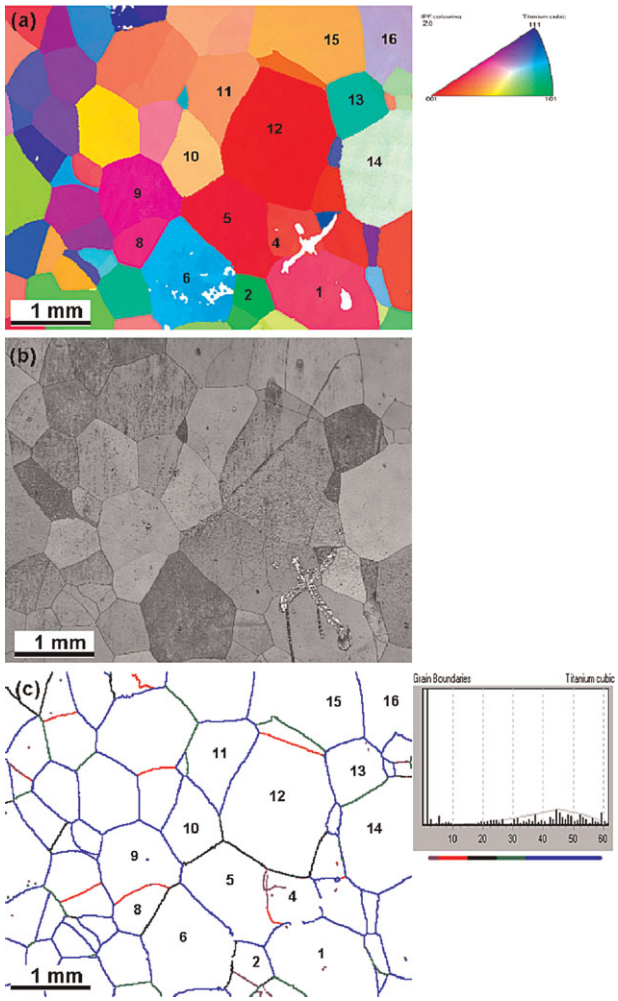

Figure 3 (online colour at: www.pss-a.com) EBSD maps; (a) inverse pole plot, (b) image quality and (c) grain boundaries of 30 at.% Nb–Ti alloy.

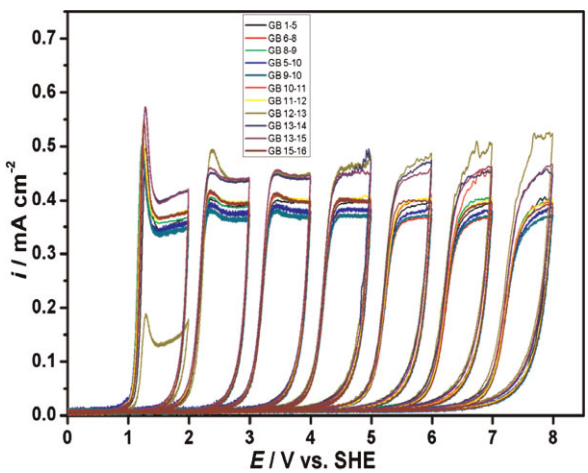

Figure 4 (online colour at: www.pss-a.com) Cyclic voltammograms from grain boundaries of 30 at.% Nb–Ti sample.

oxide growth following the development of a space charge layer as explained by the extended high field model [19]. Grain boundary 12–13 showed a much smaller current density around 150 $\mu A\,cm^{-2}$ in the second cycle compared to the other grain boundaries. This difference might be attributed to the difference in native oxide thickness between grain 12 and grain 13 with vicinal orientation of (001) and (101), respectively, which results in the formation of oxide in either of the grains only. Native oxide thickness differences were also noticed from previous work on the single grains of the same sample [13]. A current plateau is observed for all grain boundaries in the intermediate potential region which shows the sole process involved is ion transfer reaction resulting in oxide thickening at a constant rate. A delay in the kinetics of the oxide growth is observed from the smeared out increase in the current as the potential is increased. The kinetic delay is also evident from the increased gap between two successive cathodic and anodic curves as the applied potential increases [20].

Faradays law is the basis for calculating the oxide formation factor which averagely puts the amount of oxide grown per each volt applied using Eqs. (1) and (4):

$$d = \frac{Mq}{zrF\rho}, \tag{1}$$

where d is the oxide thickness, M the molecular weight, q the charge density, z number of exchanged electrons per formula unit, r the roughness factor, F the Faradays constant and ρ is the density of the mixed oxide [21]. The formation factor, inversely proportional to the electric field strength during oxide growth, calculated for each grain boundary is tabulated in Table 1. It can be calculated from a plot of the incremental charge of oxide formation against potential using Eq. (4).

3.2 Electrochemical impedance spectroscopy

The capacitive reactance from the impedance measurements will give the capacitance of the oxides based on Eq. (2):

$$\chi_c = \frac{1}{2\pi f C}, \tag{2}$$

Table 1 Summary of the oxide parameters calculated for the oxides grown on different grain boundaries of 30 at.% Nb–Ti alloy where θ is the misorientation angle.

grain boundary	θ	k/nm V^{-1}	ε_r	$N_D/10^{18}$ cm^{-3}	E_{fb}/V
8–9	5.7	2.76	77.9	5.7	−0.23
6–8	23.5	2.46	53.5	14.6	−0.25
5–10	23.9	2.62	53.8	12.0	−0.27
13–14	31.2	3.09	100.9	10.5	−0.24
13–15	42.4	3.06	101.7	66.6	−0.22
12–13	44.8	3.00	99.7	8.1	−0.26
11–12	44.9	2.76	79.9	10.4	−0.24
9–10	46.8	2.55	70.3	12.3	−0.25
15–16	46.9	2.70	78.2	11.8	−0.27
10–11	59.8	2.78	78.5	8.3	−0.24

where χ_c is capacitive reactance, f the frequency where the phase shift reaches the maximum and C is the capacitance [22, 23]. The capacitance is then related to the dielectric number of the mixed oxide grown as shown on Eq. (3) for a parallel plate condenser

$$C = \frac{\varepsilon_r \varepsilon_0}{d}, \tag{3}$$

where ε_r is the relative permittivity of the mixed oxide, ε_0 the permittivity of vacuum and d is the oxide thickness which can be expressed as in Eq. (4) for its dependence on the applied potential (E):

$$d = k(E - E_{ox}), \tag{4}$$

where E_{ox} is the equilibrium potential of the oxide electrode [20]. From the above equations the inverse capacitance can be written as:

$$\frac{1}{C} = \frac{k}{\varepsilon_r \varepsilon_0}(E - E_{ox}). \tag{5}$$

Based on Eq. (5) Fig. 5 is plotted aimed at determining the dielectric number of the oxides grown at the different grain boundaries. All the calculated values of the dielectric numbers were summarized in Table 1.

3.3 Mott–Schottky analysis

The Mott–Schottky relationship is given by:

$$C_{sc}^{-2} = \left(\frac{2}{e\varepsilon_r \varepsilon_0 N_D}\right)\left(E - E_{fb} - \frac{kT}{e}\right), \tag{6}$$

where C_{sc} capacitance of the space charge region, e is elementary electronic charge, N_D is donor concentration, E_{fb} is the flat band potential, k is the Boltzmann constant and T is temperature [24]. Based on this equation the type of the semiconductor, the charge carrier concentration and flat band potential of the oxides grown were determined. Figure

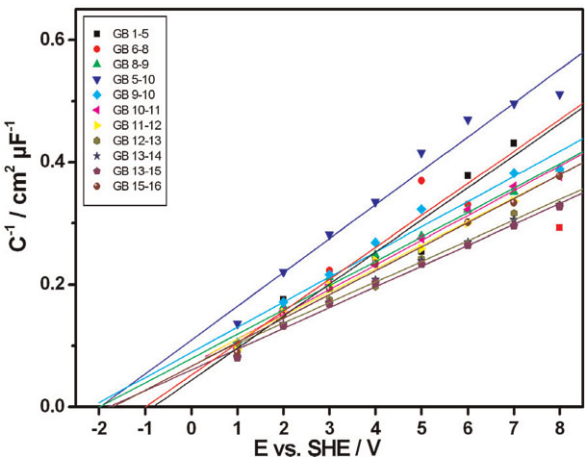

Figure 5 (online colour at: www.pss-a.com) Plot of inverse capacitance versus potential.

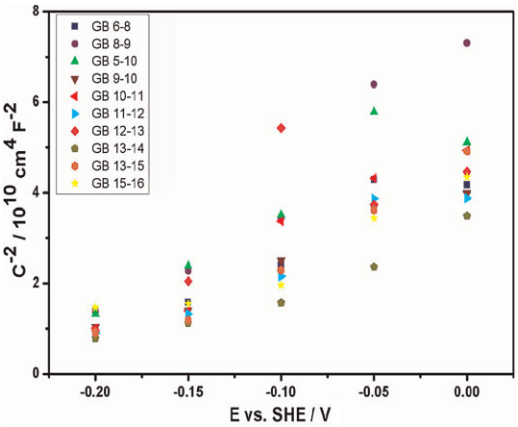

Figure 6 (online colour at: www.pss-a.com) Mott–Schottky plot for the oxides grown potentiostatically at the grain boundaries of 30 at.% Nb–Ti alloy.

6 shows the Mott–Schottky plot for oxides grown at the grain boundaries where the above measurements were carried out. All the oxides showed n-type semiconducting properties evident from the positive slope in the Mott–Schottky plot. The donor concentrations are different for different combinations of grain orientations at the grain boundaries which have different boundary angles.

Table 1 summarizes the values calculated for the formation factor (k), dielectric number (ε_r) and donor concentrations (N_D) obtained from the microelectrochemial measurements carried out at different grain boundaries of the 30 at.% Nb–Ti sample. The formation factor shows wide spread with the values reaching a value around 3 nm V^{-1}. The observed differences might be due to the additional surface area exposed to the electrolyte due to the difference in the topography of the various grains. Three types of grain geometries were observed; wall, trench and step-type examples of which are given as AFM topographies in Fig. 7. Moreover the variation in grain boundary energy with the misorientation angle induces differences in reactivity towards oxide formation among the grain boundaries. Like the formation factor the dielectric number and donor concentration varies with the grain boundaries. Presence of impurities in the grain boundary region might result in oxides having impurities/compounds of impurities besides the expected oxides of titanium and niobium. Incorporation of the impurities might change the dielectric number of the oxide and the free electron density concentration as can be seen in Table 1 for different grain boundaries of the 30 at.% Nb–Ti alloy.

Efforts were made on to make the working electrode area (1.6×10^{-5} cm^{-2}) as small as possible so that it includes only a small part from the individual grains forming the grain boundary and second to grow the oxides symmetrically across the grain boundaries. Since individual grains of the 30 at.% Nb–Ti sample dictate the values of the oxide parameters such as oxide formation factor, dielectric number and donor concentrations [13].

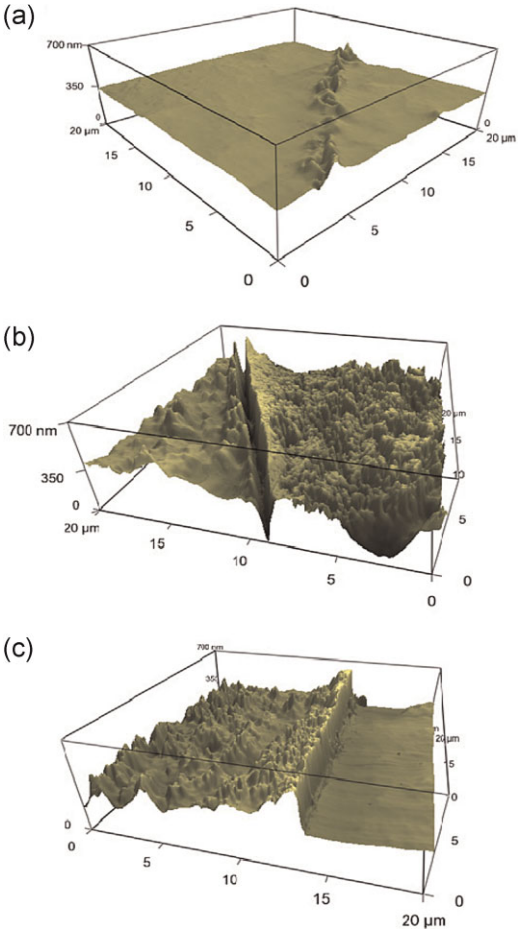

Figure 7 (online colour at: www.pss-a.com) AFM micrograph after oxide growth of grain boundary: (a) 8–9 (wall-type), (b) 13–15 (trench-type) and (c) 15–16 (step-type) of Ti-30 at.% Nb sample.

4 Summary A scanning droplet cell was used to grow oxides at the grain boundaries of a potential biomaterial 30 at.% Nb–Ti β-type titanium alloy to study the local electrochemical response and the oxide properties. The oxide spots were grown by eight cycles in the potential region of 0–8 V using cyclic voltammetry. Electrochemical impedance measurements were carried out right after the oxide growth to determine the relative permittivity of the oxide formed. No electron transfer reactions were observed during the oxide growth in all of the grain boundaries. Rather the oxide is thickening at a constant rate with the applied potential. The oxide thickness is different on different grain boundaries comprised of two grains with different crystallographic orientation for the same applied potential. Likewise the permittivity of the oxide and the donor concentration have different values for different grain boundaries of the 30 at.% Nb–Ti β-type titanium alloy.

Acknowledgements M. T. Woldemedhin acknowledges the IMPRS-SurMat for the doctoral fellowship. S. Hild and T.

Fischinger from the Institute of Polymer Sciences, Johannes Kepler University are acknowledged for the AFM measurements.

References

[1] M. A. Baker, S. L. Assis, O. Z. Higa, and I. Costa, Acta Biomater. **5**, 63 (2009).
[2] M. Karthega, V. Raman, and N. Rajendran, Acta Biomater. **3**, 1019 (2007).
[3] E. Eisenbarth, D. Velten, M. Muller, R. Thull, and J. Breme, Biomaterials **25**, 5705 (2004).
[4] D. Raabe, B. Sander, M. Friak, D. Ma, and J. Neugebauer, Acta Mater. **55**, 4475 (2007).
[5] A. Cremasco, W. R. Osorio, C. M. A. Freire, A. Garcia, and R. Caram, Electrochim. Acta **53**, 4867 (2005).
[6] C. R. M. Afonso, G. T. Aleixo, A. J. Ramirez, and R. Caram, Mater. Sci. Eng. C **27**, 908 (2007).
[7] B. Sander and D. Raabe, Mater. Sci. Eng. A **479**, 236 (2008).
[8] S. E. Kim, J. H. Son, Z. T. Hyun, H. W. Jeong, Y. T. Lee, J. S. Song, and J. H. Lee, Met. Mater. Int. **13**, 151 (2007).
[9] A. I. Mardare, A. Savan, A. Ludwig, and A. D. Wieck, Electrochim. Acta **54**, 5973 (2009).
[10] D. H. Ping, C. Y. Cui, F. X. Yin, and Y. Yamabe-Mitarai, Scr. Mater. **54**, 1305 (2006).
[11] Y. Mantani and M. Tajima, Mater. Sci. Eng. A **438**, 315 (2006).
[12] M. T. Woldemedhin, D. Raabe, and A. W. Hassel, Phys. Status Solidi A **207**, 812 (2010).
[13] M. T. Woldemedhin, D. Raabe, and A. W. Hassel (in press).
[14] S. Ramamurthy, A. Atrens, and I. O. Smith, Mater. Sci. Forum **44**, 139 (1989).
[15] H. Wise and J. Oudar, Material Concepts in Surface Reactivity and Catalysis (Dover Publications, New York, 2001), p. 162.
[16] K. Fushimi, M. Stratmann, and A. W. Hassel, Electrochim. Acta **52**, 1290 (2006).
[17] A. I. Mardare, A. D. Wieck, and A. W. Hassel, Electrochim. Acta **52**, 7865 (2007).
[18] A. W. Hassel and M. M. Lohrengel, Electrochim. Acta **42**, 3327 (1997).
[19] M. M. Lohrengel, Mater. Sci. Eng. R **11**, 243 (1993).
[20] J. W. Schultze and A. W. Hassel, in: Encyclopedia of Electrochemistry, Vol. 4, edited by A. J. Bard and M. Stratmann, Corrosion and Oxide Films, edited by M. Stratmann and G. S. Frankel (Wiley-VCH, Weinheim, 2003), pp. 216–270 and 188–189.
[21] J. W. Schultze and M. M. Lohrengel, Electrochim. Acta **45**, 2499 (2000).
[22] M. Schneider, S. Schroth, J. Schilm, and A. Michaelis, Electrochim. Acta **54**, 2663 (2009).
[23] D. Kong, S. Chen, C. Wang, and W. Yang, Corros. Sci. **45**, 747 (2003).
[24] R. Silva, M. A. Barbosa, B. Randot, and M. C. Belo, Br. Corros. J. **25**, 136 (1990).